ARTICLE

Molecular basis of photochromism of a fluorescent protein revealed by direct ^{13}C detection under laser illumination

Hideaki Mizuno · Tapas Kumar Mal ·
Markus Wälchli · Takashi Fukano ·
Mitsuhiko Ikura · Atsushi Miyawaki

Abstract Dronpa is a green fluorescent protein homologue with a photochromic property. A green laser illumination reversibly converts Dronpa from a green-emissive bright state to a non-emissive dark state, and ultraviolet illumination converts it to the bright state. We have employed solution NMR to understand the underlying molecular mechanism of the photochromism. The detail characterization of Dronpa is hindered as it is metastable in the dark state and spontaneously converts to the bright state. To circumvent this issue, we have designed in magnet laser illumination device. By combining the device with a 150-mW argon laser at 514.5 nm, we have successfully converted and maintained Dronpa in the dark state in the NMR tube by continuous illumination during the NMR experiments. We have employed direct-detection of ^{13}C nuclei from the carbon skeleton of the chromophore for detailed characterization of chromophore in both states of Dronpa by using the Bruker TCI cryoprobe. The results from NMR data have provided direct evidence of the double bond formation between C^{α} and C^{β} of Y63 in the chromophore, the β-barrel structure in solution, and the ionized and protonated state of Y63 hydroxyl group in the bright and dark states, respectively. These studies have also revealed that a part of β-barrel around the chromophore becomes polymorphic only in the dark state, which may be critical to make the fluorescence dim by increasing the contribution of non-emissive vibrational relaxation pathways.

Keywords Fluorescent protein · Photochromism · Polymorphism · In magnet laser illumination · ^{13}C direct-detection

H. Mizuno (✉) · T. Fukano · A. Miyawaki (✉)
Cell Function and Dynamics, Brain Science Institute, RIKEN,
2-1 Hirosawa, Wako-city, Saitama 351-0198, Japan
e-mail: hideaki.mizuno@chem.kuleuven.be

A. Miyawaki
e-mail: matsushi@brain.riken.jp

T. K. Mal · M. Ikura
Division of Signaling Biology, Ontario Cancer Institute
and Department of Medical Biophysics, University of Toronto,
MaRS Toronto Medical Dicovery Tower, Room 4-804,
101 College Street, Toronto, ON M5G 1L7, Canada

M. Wälchli
Bruker BioSpin K.K, 3-21-5, Ninomiya, Tsukuba-city,
Ibaraki 305-0051, Japan

Present Address:
H. Mizuno
Department of Chemistry and INPAC, Katholieke Universiteit
Leuven, Celestijnenlaan 200F, 3001 Heverlee, Belgium

T. K. Mal
Pfizer Research, 200 Cambridgepark Drive, Cambridge,
MA 02140, USA

Introduction

Dronpa is a photochromic fluorescent protein made by genetic engineering based on a homologue of green fluorescent protein (GFP) isolated from a Pectiniidae species (Ando et al. 2004). Dronpa emits green fluorescence efficiently ($\phi_{fl} = 0.85$) with absorption and emission maxima of 503 and 518 nm, respectively. The absorption at 503 nm also converts Dronpa to a non-emissive 'dark state', but the quantum efficiency of the switching is three orders of magnitude lower than the fluorescent emission ($\phi_{sw} = 0.00032$). In the dark state, Dronpa absorbs ultraviolet light with an absorption maximum of 390 nm, which efficiently converts Dronpa back to the original 'bright state'

($\phi_{sw} = 0.37$). This reversible photoswitching behavior of Dronpa has been exploited to analyze dynamic aspects of protein localization in cells, for example the nucleoplasmic shuttling of mitogen-activated protein kinase and NF-AT (Kwon et al. 2008; Ando et al. 2004). Recently, Dronpa has also been used as a fluorophore for subdiffraction microscopy including photoactivation localization microscopy (PALM) (Mizuno et al. 2010; Flors et al. 2007; Shroff et al. 2007) and photoswitching microscopy (Dedecker et al. 2007). Crystal structures of Dronpa in the bright state have been reported both by our laboratory and others (Mizuno et al. 2008; Nam et al. 2007; Stiel et al. 2007; Wilmann et al. 2006). Like other fluorescent proteins, the overall fold of Dronpa is a β-barrel structure containing 11 β-strands, in which the chromophore is found in the cis configuration. The chromophore was found in the trans configuration in the dark state of Dronpa (Andresen et al. 2007), suggesting that the cis–trans photoisomerization is a critical reaction for the photochromism. X-Ray crystallography can provide detailed structural information for a crystal under cryogenic conditions, however photochemical processes are affected by thermodynamic properties. Thus we have employed NMR spectroscopy to understand the molecular mechanisms of the photochromism of Dronpa.

The bright state of Dronpa is stable, but the dark state is metastable and gradually returns to the bright state in several hours even in the absence of UV light. Therefore, continuous illumination of the NMR sample is required for long NMR data acquisition in the dark state. Laser beam illumination in the magnet has been combined with NMR acquisition to improve the sensitivity of NMR, which is known as photochemically induced dynamic nuclear polarization (photo-CIDNP) (Bargon et al. 1967; Ward and Lawler 1967). Two methods have been reported to introduce laser beam to the magnet for photo-CIDNAP (Mok and Hore 2004). One is a cylindrical quartz rod placed in the NMR probe (Kaptein 1982). This method requires modification of the NMR probe and assembly of an optical set to guide the light to the rod. The other method makes use of an optic fiber, which is introduced to the sample through the magnet bore. The tip of the fiber is immersed into the sample (Mok and Hore 2004), mounted in a coaxial insert (Scheffler et al. 1985), or coupled to a special quartz rod with a conical tip that is inserted into the NMR tube (Kuhn and Schwalbe 2000). Such fiber-coupled illumination has been applied to NMR acquisition of photoactive yellow protein (Craven et al. 2000; Rubinstenn et al. 1998, 1999) and phototropin (Harper et al. 2003, 2004). In this work, we designed and built a simple laser illumination device composed of a multimode optic fiber and two objective lenses. The tip of the fiber was immersed in a water-filled glass insert of a symmetric Shigemi NMR tube.

Laser illumination of Dronpa with this device successfully kept it in the dark state during the NMR data acquisitions.

Inverse ^{1}H-detecting NMR experiments are conventionally used for observation of heteronuclei such as ^{13}C and ^{15}N in proteins because of the high sensitivity of ^{1}H-nucleus detection due to the large gyromagnetic ratio of ^{1}H. However, spectra acquired with these protocols provide limited information on the chromophore of Dronpa, since four hydrogen atoms (H^N, $H^{C\alpha}$, and one of $H^{C\beta}$ of Y63, and H^N of G64) are abstracted to form the chromophore by cyclization, dehydration, and reduction of three amino acid residues, C62–Y63–G64 (Fig. 2e). We took advantage of recent advancements in ^{13}C-direct detection (Bertini et al. 2004; Bermel et al. 2008) using Bruker TCI cyoprobe to characterize ^{13}C nuclei of Y63, the central residue of the chromophore.

Materials and methods

Production of [^{13}C, ^{15}N]-enriched Dronpa

Escherichia coli BL21(DE3) was transformed with pET28a/Dronpa (Mizuno et al. 2008) and grown at room temperature in M9 media containing glucose-^{13}C$_6$ (1 mg/ml, Cambridge Isotope) and ^{15}NH$_4$Cl (2 mg/ml, Taiyo Nippon Sanso) as exclusive carbon and nitrogen sources, respectively. Production of Dronpa was induced with 100 μM isopropyl β-D-thiogalactoside (IPTG, Nakarai Tesque) at an OD_{600} of 0.71. Following additional 14-h incubation, bacteria were harvested by centrifugation (3,000g, 10 min) and resuspended in phosphate buffered saline (PBS). Bacteria were disrupted by repeated freezing/thawing in the presence of lysozyme (250 μg/ml, Sigma–Aldrich), DNaseI (250 μg/ml, Sigma–Aldrich), 1 mM MgCl$_2$, and proteinase inhibitors (10 μM E-64, 10 μM leupeptin, 1 μM pepstatin A, Peptide Institute; 50 μM phenylmethylsulfonyl fluoride, Calbiochem). Bacterial debris was removed by centrifugation (9,000g, 10 min) and Dronpa was purified from the supernatant as described below.

Production of Tyr-^{13}C$_9$,^{15}N-labeled Dronpa

Specific labeling of tyrosine residues of Dronpa was carried out by in vitro translation (RTS 500 ProteoMaster E. coli kit, Roche) in the presence of GroE supplement (Roche). Amino acid mixture for the reaction was prepared with RTS Amino Acid Sampler (Roche) and Tyr-^{13}C$_9$,^{15}N (Isotec). The chromophore maturation requires molecular oxygen, however the RTS system has been designed to react under anaerobic conditions. Thus after the 24-h translation reaction, the product (5 ml in total) was

transferred to a 50-ml closed cap test tube and incubated for 5 h under gentle mixing to allow the maturation. Dronpa was then purified from the supernatant as described below.

Preparation of the NMR sample

Proteins were purified using Ni–NTA agarose (Qiagen). The histidine tag was removed by thrombin treatment (Novagen) according to the manufacturer's manual, and the cleaved tag and any remaining uncleaved protein were removed by passage through a Ni–NTA agarose column. The buffer was exchanged to a buffer for NMR measurement (20 mM phosphate buffer, pH 7.5, containing 50 mM NaCl) with a desalting column (PD-10, GE Healthcare). The protein solution was concentrated to 2.3 mM ([^{13}C,^{15}N]-enriched Dronpa) or 0.5 mM (Tyr-^{13}C$_9$, ^{15}N-labeled Dronpa) by ultrafiltration (Centricon YM-30, Amicon) and supplemented with D$_2$O to a final concentration of 2%.

NMR recording

All the NMR data were recorded at 27°C by using a Bruker AVANCE 600-MHz spectrometer equipped with a TCI cryoprobe. Sequential resonance assignments for backbone $^1H^N$, $^{13}C^\alpha$, $^{13}C^\beta$, and ^{15}N nuclei were accomplished using two dimensional ^{15}N-^{1}H HSQC and three dimensional HNCACB and CBCACONH dataset of [^{13}C,^{15}N]-enriched Dronpa. Topspin (Bruker BioSpin) and CARA (www.nmr.ch) were used to process and analyze the data. Secondary structure was calculated using modified weighted chemical shift indices (CSI) as described elsewhere (Mal et al. 2004; Spera and Bax 1991; Wishart and Sykes 1994).

Relaxation data measurement

Sensitivity enhanced heteronuclear NMR experiments, T_2 and {^{1}H}–^{15}N nuclear Overhauser effect (NOE) (Farrow et al. 1994; Akke and Palmer 1996) were recorded. ^{15}N T_2
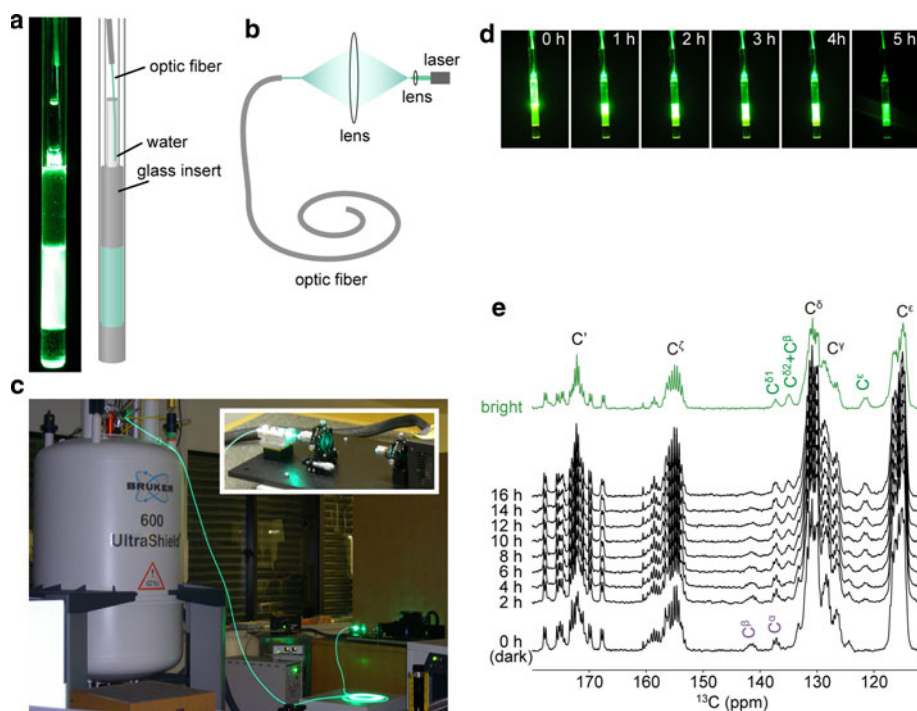

Fig. 1 In magnet laser illumination device. **a** A picture and illustration of the device around the sample tube. The Dronpa solution was placed in a 5-mm symmetrical Shigemi NMR tube and the glass-insert of the tube was set on the top of the protein solution. A small amount of water was poured in the glass-insert and the tip of the optic fiber was immersed in the water. **b** Coupling of the argon laser to the optic fiber using two objective lenses. **c** Overview picture of the illumination device. *Inset* is a picture of the assembly of the optical components to couple the laser to the fiber. **d** Laser illumination of the Dronpa solution in the Shigemi NMR tube. The

laser illuminated the sample continuously and images were taken every hour using a digital camera (ISO 100, F 4.8, 1/200; Camedia C-5060; Olympus). **e** Spontaneous dark-to-bright conversion of Dronpa during NMR recording in the dark. A one-dimensional ^{13}C spectrum of Tyr-^{13}C$_9$,^{15}N-labeled Dronpa in the bright state was acquired before illumination (*green*). After illumination of the sample to convert it to the dark state, the laser was turned off and spectra were acquired every 2 h (*black*). Peaks assignable to Y63 were indicated in *green* and *purple* for the bright and dark state, respectively, whereas peaks for other tyrosine residues are in *black*

values were measured from ^{15}N–^1H HSQC spectra recorded with relaxation-delay times of 0.000, 16.032, 32.064, 48.094, 64.128, 80.160, 96.192, 112.224, 128.256, 144.288, 160.320, and 176.352 ms. Peak intensities were obtained using CARA. T_2 values for each residue were obtained by least-square fitting of the intensities to a mono-exponential decay function:

$$I(t) = I_0 \cdot e^{-t/T_2}$$

where I_0 is the initial peak intensity, t is the delay time and T_2 is the relaxation time constant.

Results and discussion

Development of in magnet laser illumination device

To characterize the metastable dark state of Dronpa by NMR, we built a device to illuminate the sample in the magnet during data collection (Fig. 1). Optical components that couple the laser to the fiber were assembled on an aluminum base plate. A beam from a 150-mW argon laser was expanded with a 10× objective lens (M10/NA0.25, Olympus) and focused with a long working distance 10× objective lens

Fig. 2 Backbone assignment of Dronpa. **a, b** ^{15}N–^1H HSQC spectra of [^{13}C,^{15}N]-enriched Dronpa in the bright (**a**) and dark (**b**) states. **c** ^{15}N–^1H HSQC spectra of Tyr-$^{13}C_9$,^{15}N-labeled Dronpa in *green* and *black* for the bright and dark states, respectively. Assignments are indicated with *single letter* amino acid codes with the residue numbers. The chemical shift assignments of Dronpa in the bright and dark states were deposited in the BioMagResBank (www.bmrb.wisc.edu) under the accession numbers 17162 and 17163, respectively. **d** Polymorphic region in the dark state mapped on a crystal structure (PDB ID: 2Z1O). Overall structure is shown with the *cartoon format*, and the chromophore is with the *line format*. The carbon, oxygen, and nitrogen atoms of the chromophore are in *green*, *red*, and *orange*, respectively. The polymorphic regions are highlighted with *magenta*. **e** Chromophore formation of Dronpa. The chromophore is composed of three amino acids: C62 (drawn in *cyan*), Y63 (*green*), and G64 (*magenta*). All hydrogen atoms of Y63 are shown. *Arrows* indicate hydrogen atoms abstracted upon the chromophore formation
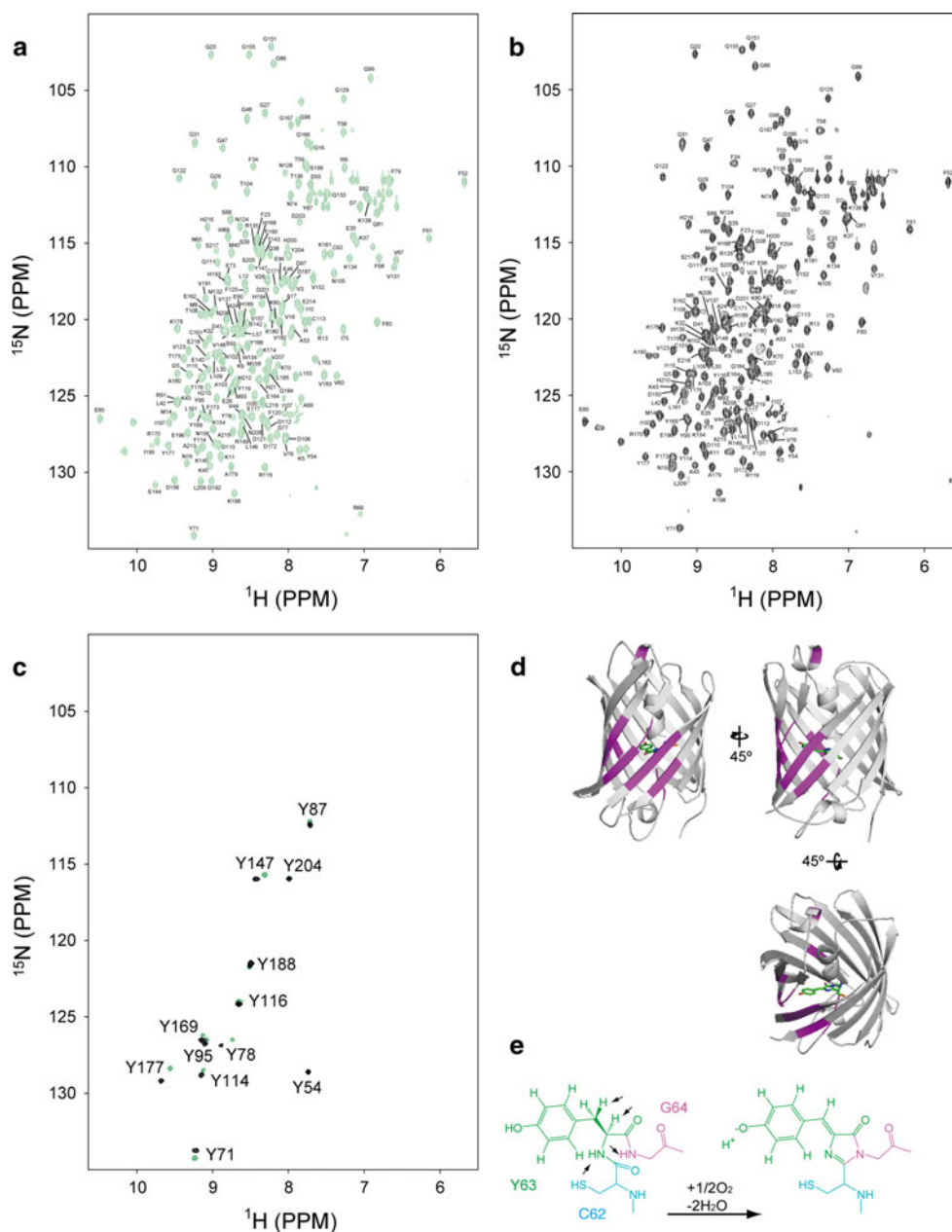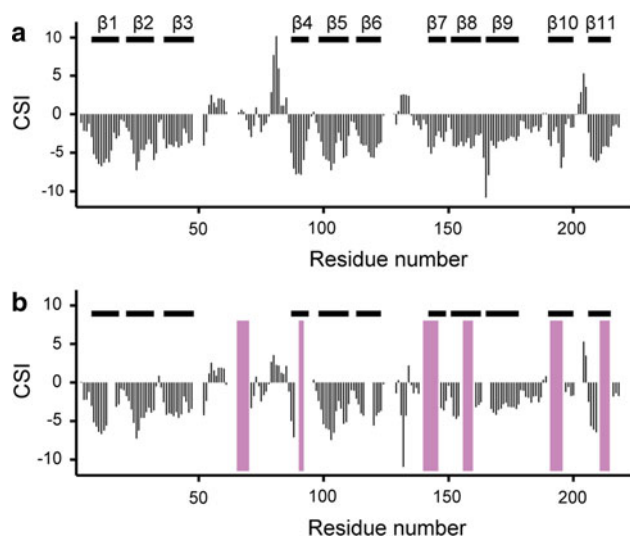
Fig. 3 Secondary structural analysis of Dronpa. $^{13}C^{\alpha}$–$^{13}C^{\beta}$ chemical shift indexes (CSI) plots of Dronpa in the bright (**a**) and dark (**b**) states are shown. *Black bars* on the top indicate β-strand regions predicted from the CSI calculation. The polymorphic regions in the dark state are highlighted with *magenta*

(MDPlan 10/NA0.25, Olympus) to one end of a multimode optic fiber (V50-MM, graded index, core diameter of 50 μm, Suruga Seiki) fixed on a fiber holder (F260, Suruga Seiki). We chose a focusing lens with NA value of 0.25, which is slightly larger than the NA value of the fiber (0.22) to introduce the focused light efficiently. The long working

distance of the lens gives enough space to adjust the focal position of the light to the fiber. The power emitted from the fiber was 85 mW, which corresponded to 55% of the input to the fiber. Since the 20 m long fiber is flexible, it is easy to introduce the other end of the fiber in the NMR magnet. Here we used 150 mW of the input power, but it can be increased to 1 W or more due to less photo-damage of multimode optic fibers than single-mode ones; the large core diameter of the multimode optic fiber (50 μm) reduces the power density of the light in the fiber. We used only single laser, but the fiber is thin (clad diameter of 125 μm) and multiple fibers can be put together to introduce multiple lines of lasers with different wavelength and/or same wavelength to increase illumination power. Power and duration of the illumination can be designed and synchronized to NMR protocols by installing TTL-driven optical components and triggering them from an NMR console.

The Dronpa protein sample was prepared in a symmetric Shigemi NMR tube (BMS-3, Shigemi). We first tried illuminating the sample with an optic fiber placed in the glass-insert of the Shigemi tube, but this was inefficient due to light scattering caused by the large refractive index difference between the fiber and the air. By pouring a small volume of water into the glass insert and immersing the end of fiber in the water, the apparent fiber-emitting angle was reduced and the laser beam was successfully introduced to the Dronpa solution (Fig. 1a).

Fig. 4 ^{15}N-backbone relaxation measurements. **a** Fitting of the signal intensity as a mono-exponential function of the relaxation-delay. Data for the residue C62 in the bright state were shown as an example. The T_2 values were calculated from the fitting. T_2 (**b**, **c**) and NOE (**d**, **e**) plots of Dronpa in the bright (**b**, **d**) and dark (**c**, **e**) states. In (**c**) and (**e**), the polymorphic regions in the dark state are highlighted with *magenta*
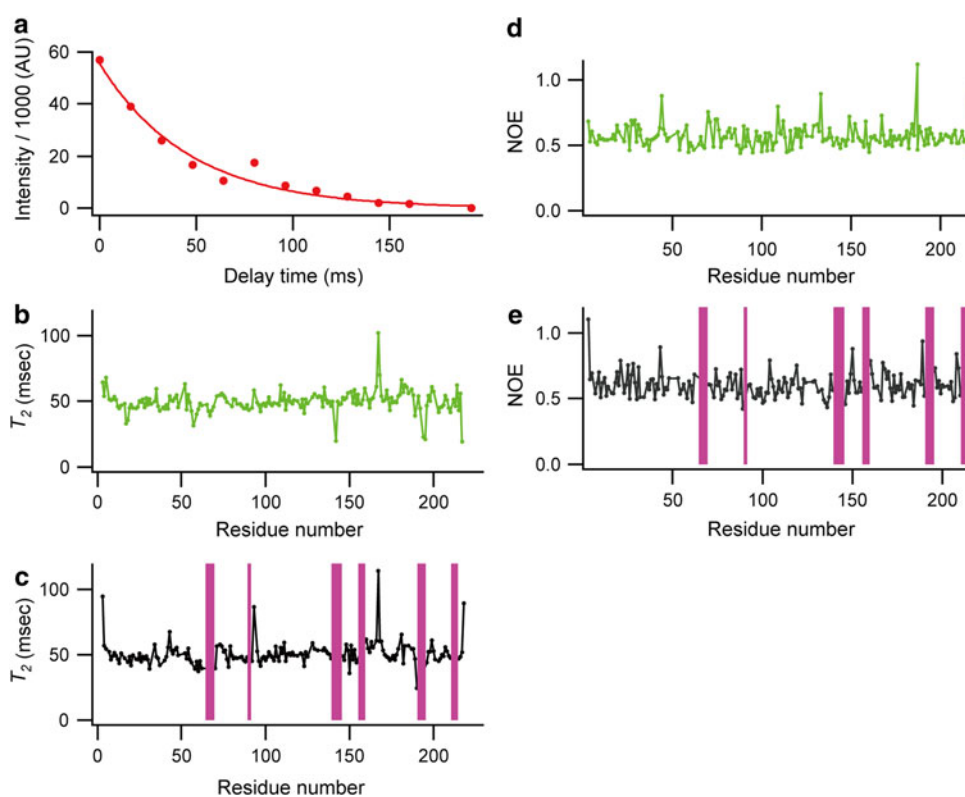
Conversion of the Dronpa sample to the dark state occurred over several hours starting at the top of the tube and progressing to the bottom (Fig. 1d from left to right). Initially, the laser illuminated only the top few mm of the solution due to a strong internal shielding effect caused by absorption of light by the concentrated Dronpa solution (Fig. 1d, left panel). The internal shielding effect was gradually reduced as Dronpa was converted to the dark state, which does not absorb light at 514.5 nm, thus allowing the laser to penetrate more deeply with time. After 5 h of continuous illumination, the Dronpa solution was completely converted to the dark state (Fig. 1d, right panel) which was maintained during the NMR experiments.

We evaluated the reversibility of the dark state of Dronpa by recording one-dimensional ^{13}C spectra of Tyr-$^{13}C_9,^{15}N$-labeled Dronpa using a Bruker TCI cryoprobe (Fig. 1e). The spectrum for the bright state was acquired prior to the laser illumination (a green trace). After the complete conversion of Dronpa to the dark state by the laser illumination, the laser was turned off and spectra were acquired every 2 h (black traces). The first spectrum at 0 h represents the dark state, and successive spectra reflect the gradual recovery to the bright state. The spectrum collected at 16 h was almost same as that of the bright state, indicating that majority of Dronpa in the dark state had converted to the bright state. This signifies the requirement for a continuous illumination system to maintain the dark state during the long NMR data acquisition (several hours or longer). No significant photodamage was observed during the NMR recording under the continuous laser illumination; the sample went back to the bright state upon UV illumination after the recording, and no differences were apparent in the ^{15}N-HSQC spectra upon the laser illumination (data not shown).

Backbone assignment

We first acquired the ^{15}N–^1H HSQC spectra of [$^{13}C,^{15}N$]-enriched and only Tyr-$^{13}C_9,^{15}N$-labeled Dronpa both in the bright and dark states (Fig. 2) to check protein integrity. For sequential backbone assignment, we collected HNCACB and CBCACONH data using [$^{13}C,^{15}N$]-enriched Dronpa and performed assignments of backbone $^1H^N$, $^{13}C^\alpha$, $^{13}C^\beta$ and ^{15}N atoms. There were no peaks corresponding to two of three residues in the chromophore (Y63 and G64), since these two residues lack $^1H^N$ nuclei due to abstraction of H^N atoms in the process of the chromophore formation (Fig. 2e). Backbone nuclei of total 195 amino acid residues were assigned in the bright state, which corresponded to 92.9% of the whole protein (proline residues, Y63 and G64 were excluded from the calculation). In the dark state, backbone nuclei were assigned for 171 amino acid
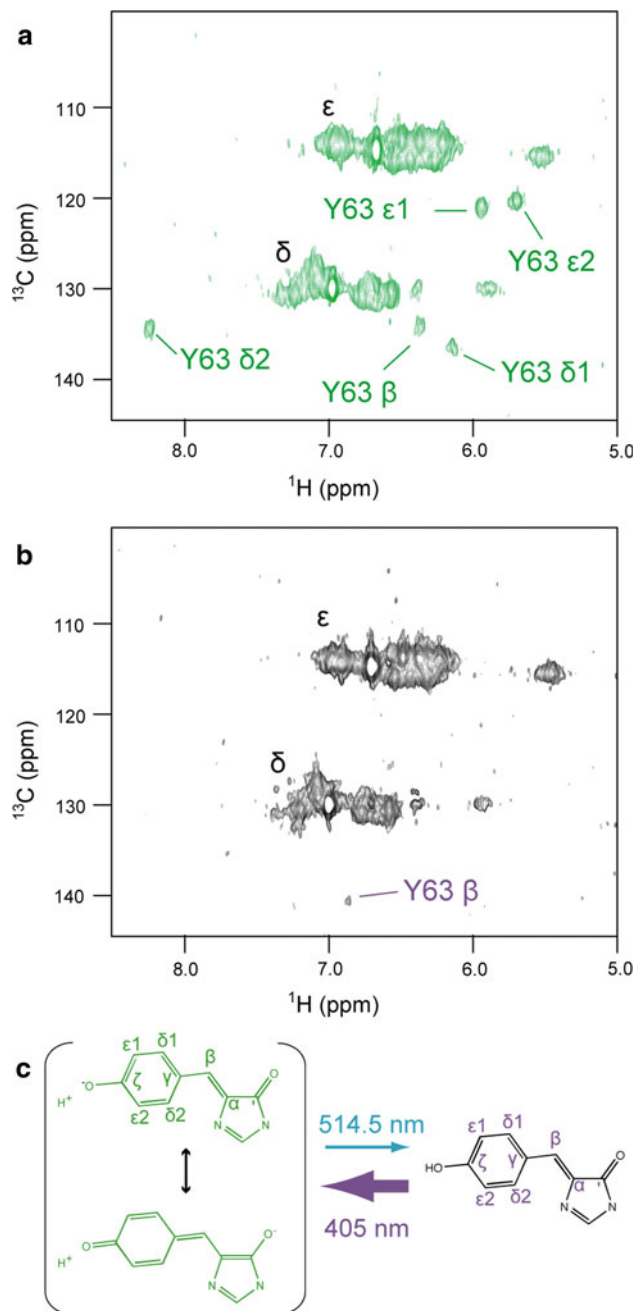

Fig. 5 ^{13}C–^1H HSQC spectra of Tyr-$^{13}C_9,^{15}N$-labeled Dronpa in the bright (**a**) and dark (**b**) states. Only the aromatic region is shown. Peaks assignable to Y63 in the bright and dark states are indicated with *green* and *purple letters*, respectively. Peaks for other tyrosine residues are in *black letters*. **c** Light-induced chromophore deprotonation/protonation responsible for the conversion between the bright and dark states

residues, corresponding to 81.4% of the whole protein. Twenty-five amino acid residues assigned in the bright state were not detected in the dark state (N65, R66, V67, F68, A69, E90, R91, P132, E140, S142, T143, E144, K145, D156, V157, N158, M159, V191, D192, H193, H914, I195, H212, A213, and E214). When mapped on the crystal
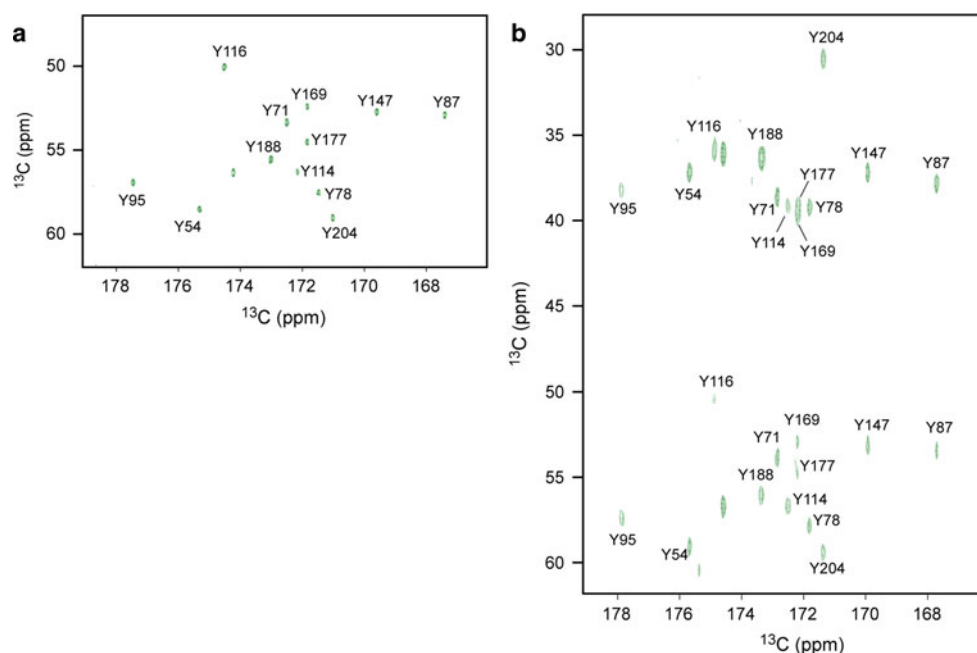
structure of Dronpa, these residues were located on strands $\beta4$, $\beta7$, $\beta8$, $\beta10$, and $\beta11$, and clustered around the side chain of the chromophore Y63, the central residue of the chromophore (Fig. 2d).

Secondary structure

The secondary structure of Dronpa was analyzed using modified weighted chemical shift indices (CSI) plot (Fig. 3) (Mal et al. 2004; Spera and Bax 1991; Wishart and Sykes 1994). Dronpa composed of 11 β-strands, which is consistent with the β-barrel structure revealed by the crystal structure (Mizuno et al. 2008; Nam et al. 2007; Stiel et al. 2007; Wilmann et al. 2006). No significant differences were observed in the secondary structural elements between the bright and dark states, indicating that Dronpa forms a β-barrel structure in solution both in the bright and dark states.

Backbone dynamics

We employed ^{15}N-backbone relaxation measurements to probe if there were any differences of conformational dynamics in the β-barrel structure between the two states of Dronpa. ^{15}N T_2 and $\{^1H\}$–^{15}N NOE (Farrow et al. 1994; Akke and Palmer III 1996) were shown (Fig 4) for the both states of [$^{13}C,^{15}N$]-enriched Dronpa. T_2 values could not be determined for undetected residues or for overlapped resonances in the ^{15}N–^1H HSQC spectra. T_2 values reported here were for 181 and 159 residues representing 80.8% and 71.0% for bright and dark states, respectively. We did not observe any major differences in the T_2 or NOE values for

these residues between the two states of Dronpa, implying that there were no significant differences in the dynamical behavior of the β-barrel structure with the exception of the region that was undetectable in the dark state (the magenta region shown in Fig. 2d).

Missing resonances in this region provided an evidence of the structural polymorphism that caused unexpected line broadening in the dark state. In the bright state, in contrast, T_2 and NOE values of residues in this region showed no significant differences from other parts of the protein, indicating that this region is rigid in the bright state. However, this region exhibits conformational heterogeneity in the dark state, suggesting that illumination creates a dynamic polymorphic state that may be responsible for the switching of the fluorescence.

Characterization of the chromophore tyrosine

To characterize the central residue of the chromophore, Y63, we first recorded ^{13}C–^1H HSQC spectra of the Tyr-U-$^{13}C,^{15}N$-labeled Dronpa (Fig. 5). The cross peak corresponding to C^β–H^β correlation of Y63 was observed in the aromatic region but not in the aliphatic region. No peak corresponding to C^α–H^α correlation of Y63 was observed. These NMR observations provided evidence of abstraction of H^α and one of the H^β atoms of Y63 followed by the formation of double bond between C^α and C^β to form the chromophore, consistent with the chromophore sutructure of 4-(*p*-hydroxybenzylidene)-5-imidazolinone (Fig. 2e).

In the bright state, the correlation peaks for C^δ–H^δ and C^ε–H^ε of Y63 were distinct from other tyrosine residues in the ^{13}C–^1H HSQC spectrum (Fig. 5a). All C^δ and C^ε of
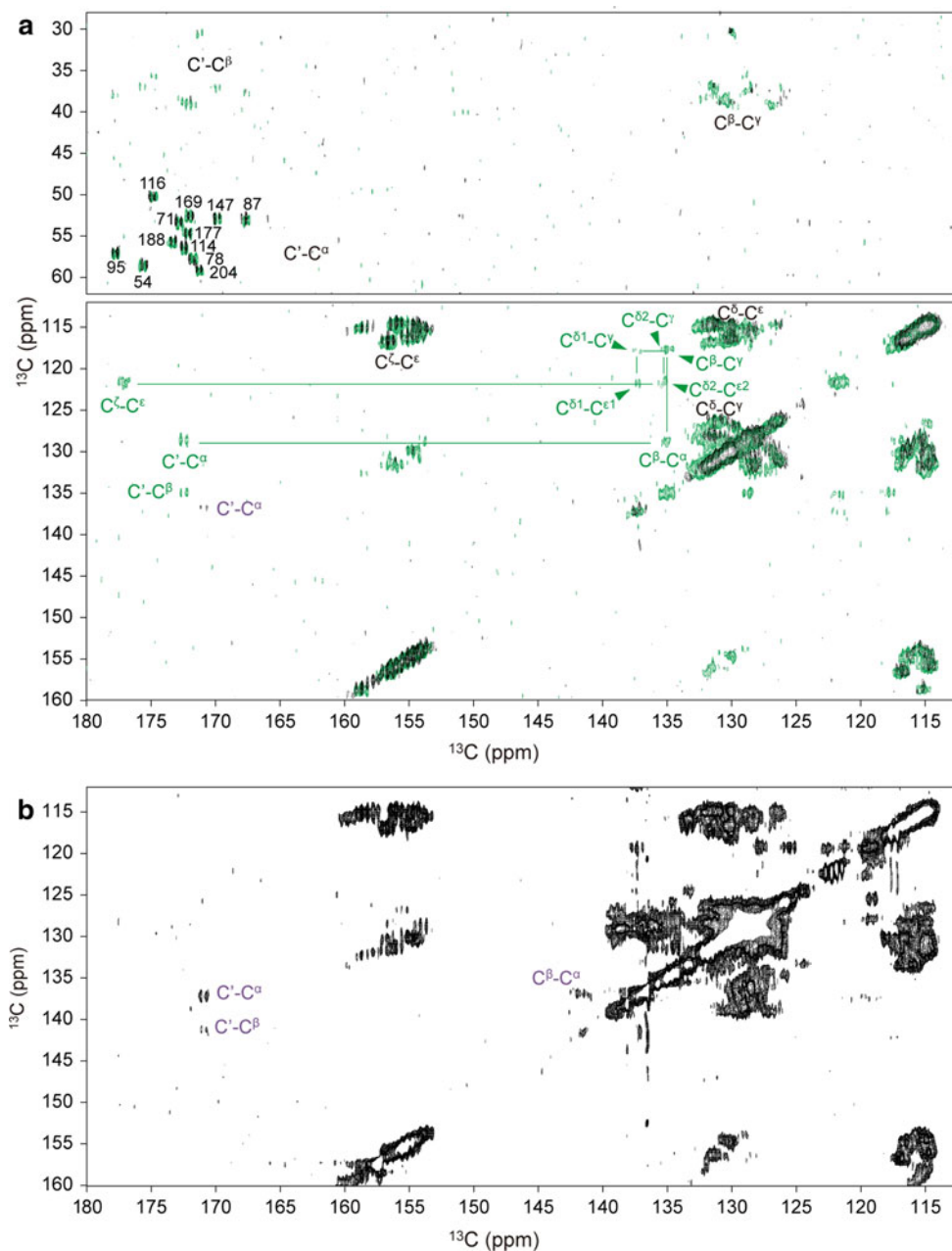
Fig. 7 ^{13}C–^{13}C NOESY spectra of Tyr-$^{13}C_9$,^{15}N-labeled Dronpa (**a**) and [^{13}C,^{15}N]-enriched Dronpa (**b**) in the bright (*green*) and dark (*black*) states. Peaks assignable to Y63 were indicated with *green* (for the bright state) and *purple* (for the dark state) *letters*. Peaks for other tyrosine residues are in *black letters*

Y63 showed downfield shifts, and one of H^δ ($H^{\delta 1}$) and two H^ε showed upfield shifts. These results are consistent with deprotonation of O^η (Bradbury and Ramesh 1985; Egan et al. 1978; Wilbur and Allerhand 1976). The other H^δ ($H^{\delta 2}$) showed a downfield shift, which was apparently caused by the ring current effect of the chromophore imidazolinone ring. This proton–ring interaction revealed a *cis* co-planar conformation of the bright-state chromophore, consistent with the crystal structures (Mizuno et al. 2008;

Nam et al. 2007; Stiel et al. 2007; Wilmann et al. 2006). In the bright state, ^{13}C and ^1H nuclei at positions $\delta 1$ and $\delta 2$ as well as $\varepsilon 1$ and $\varepsilon 2$ had different chemical shift values, indicating that the environment of these nuclei were different and the chromophore hydroxyphenyl group could not rotate freely. In the dark state, the correlation peaks for C^δ–H^δ and C^ε–H^ε of Y63 were indistinguishable from other tyrosine residues (Fig. 5b), indicating the protonation of O^η and a non *cis* co-planar conformation of the chromophore.

Direct ^{13}C detection for the chromophore analyses

For detailed analyses of the chromophore, we employed direct ^{13}C detection experiments on Tyr-^{13}C$_9$,^{15}N-labeled Dronpa. We first acquired the CACO spectrum of Dronpa in the bright state (Fig. 6a) to determine whether it is possible to observe signals from tyrosine residues. ^{13}C$^\alpha$–^{13}C' correlation peaks corresponding to all tyrosine residues except Y63 were observed in the usual chemical shift values of ^{13}C$^\alpha$ between 49 and 60 ppm. In the CBCACO spectra, ^{13}C$^\beta$–^{13}C' as well as ^{13}C$^\alpha$–^{13}C' correlations were observed for all tyrosine residues except Y63 in the usual ^{13}C$^\beta$ chemical shift region between 30 and 40 ppm (Fig. 6b).

Figure 7a shows ^{13}C–^{13}C NOESY spectra of Tyr-^{13}C$_9$,^{15}N-labeled Dronpa both in the bright and dark states. Chemical shifts of Y63 ^{13}C nuclei are summarized in Table 1. In the bright state, peaks corresponding to all ^{13}C–^{13}C one-bond correlations of Y63 of Dronpa were observed at positions different from those of other tyrosine residues. ^{13}C$^\alpha$ and ^{13}C$^\beta$ of Y63 showed a downfield shift to the aromatic region at 128.5 and 134.8 ppm, respectively, which is consistent with double bond formation between these atoms upon the chromophore formation. C$^\zeta$ shows a downfield shift to 177.0 ppm, which gives NMR evidence for deprotonation of O$^\eta$ in the bright state (Egan et al. 1978; Wilbur and Allerhand 1976).

In the dark state, only a weak peak corresponding to C$^\alpha$–C' was detected for Y63 in the ^{13}C–^{13}C NOESY spectrum. The concentration of Tyr-^{13}C$_9$,^{15}N-labeled Dronpa was relatively low (0.5 mM) due to the limitations of the in vitro translation system. To improve sensitivity, we used [^{13}C,^{15}N]-enriched Dronpa expressed in E. coli; the expression in E. coli allowed us to prepare a 2.3 mM sample (Fig. 7b). Although all residues were ^{13}C-enriched, peaks corresponding to C$^\alpha$–C', C$^\alpha$–C$^\beta$, and C$^\beta$–C' of Y63

were isolated due to large downfield shifts of ^{13}C$^\alpha$ and ^{13}C$^\beta$ to 136.9 and 140.8 ppm, respectively. No other resonance signals of Y63 carbons were distinct from those of the other tyrosine residues in the spectrum, which is consistent with the protonation of O$^\eta$ in the dark state.

Conclusion

The laser illumination device successfully introduced the laser beam to the sample in the NMR tube during long NMR experiments, and made it possible to acquire NMR data that require long acquisition times, such as triple resonance and ^{13}C direct-detection experiments. With this illumination device we are able to make detail characterization of the metastable dark state of Dronpa. Together with the direct ^{13}C detection and traditional proton-based NMR experiments, we have fully characterized the chromophore in both states of Dronpa. These studies revealed structural aspects of Dronpa responsible for the photochromism such as chromophore structure, ionization state, and dynamics of the β-barrel.

References

Akke M, Palmer AG III (1996) Monitoring macromolecular motions on microsecond to millisecond time scales by R$_{1\rho}$–R$_1$ constant relaxation time NMR spectroscopy. J Am Chem Soc 118: 911–912

Ando R, Mizuno H, Miyawaki A (2004) Regulated fast nucleocytoplasmic shuttling observed by reversible protein highlighting. Science 306:1370–1373

Andresen M, Stiel AC, Trowitzsch S, Weber G, Eggeling C, Wahl MC, Hell SW, Jakobs S (2007) Structural basis for reversible photoswitching in Dronpa. Proc Natl Acad Sci USA 104: 13005–13009

Bargon J, Fisher H, Johnsen U (1967) Kernresonanz-emissionslinein wahrend rascher radikalreaktionen. I. aufnahmeverfahren und beispiele. Z Naturforsch A22:1551–1555

Bermel W, Felli IC, Kümmerle R, Pierattelli R (2008) ^{13}C Direct-detection biomolecular NMR. Concepts Magn Reson 32A: 183–200

Bertini I, Felli IC, Kümmerle R, Moskau D, Pierattelli R (2004) ^{13}C–^{13}C NOESY: an attractive alternative for studying large macromolecules. J Am Chem Soc 126:464–465

Bradbury JH, Ramesh V (1985) ^{1}H n.m.r. studies of insulin. Assignment of resonances and properties of tyrosine residues. Biochem J 229:731–737

Table 1 Chemical shifts of ^{13}C nuclei of tyrosine residues

	Y63 (ppm)		Other tyrosine residues (ppm)
	Bright	Dark	
^{13}C'	172.4	170.9	167–179
^{13}C$^\alpha$	128.5	136.9	49–60
^{13}C$^\beta$	134.8	140.8	30–40
^{13}C$^\gamma$	117.9	ND[a]	125–132
^{13}C$^{\delta 1}$	137.3	ND	124–133
^{13}C$^{\delta 2}$	135.4	ND	124–133
^{13}C$^{\epsilon 1}$	122.0	ND	113–118
^{13}C$^{\epsilon 2}$	121.2	ND	113–118
^{13}C$^\zeta$	177.0	ND	153–160

[a] ND not determined

Craven CJ, Derix NM, Hendriks J, Boelens R, Hellingwerf KJ, Kaptein R (2000) Probing the nature of the blue-shifted intermediate of photoactive yellow protein in solution by NMR: hydrogen–deuterium exchange data and pH studies. Biochemistry 39:14392–14399

Dedecker P, Hotta J, Flors C, Sliwa M, Uji-I H, Roeffaers MB, Ando R, Mizuno H, Miyawaki A, Hofkens J (2007) Subdiffraction imaging through the selective donut-mode depletion of thermally stable photoswitchable fluorophores: numerical analysis and application to the fluorescent protein Dronpa. J Am Chem Soc 129:16132–16141

Egan W, Shindo H, Cohen JS (1978) On the tyrosine residues of ribonuclease A. J Biol Chem 253:16–17

Farrow NA, Muhandiram R, Singer AU, Pascal SM, Kay CM, Gish G, Shoelson SE, Pawson T, Forman-Kay JD, Kay LE (1994) Backbone dynamics of a free and phosphopeptide-complexed Src homology 2 domain studied by ^{15}N NMR relaxation. Biochemistry 33:5984–6003

Flors C, Hotta J, Uji-I H, Dedecker P, Ando R, Mizuno H, Miyawaki A, Hofkens J (2007) A stroboscopic approach for fast photoactivation-localization microscopy with Dronpa mutants. J Am Chem Soc 129:13970–13977

Harper SM, Neil LC, Gardner KH (2003) Structural basis of a phototropin light switch. Science 301:1541–1544

Harper SM, Neil LC, Day IJ, Hore PJ, Gardner KH (2004) Conformational changes in a photosensory LOV domain monitored by time-resolved NMR spectroscopy. J Am Chem Soc 126:3390–3391

Kaptein R (1982) In: Berliner LJ, Reuben J (eds) Biological magnetic resonance, vol 4. Plenum Press, New York, pp 145–191

Kuhn T, Schwalbe H (2000) Monitoring the kinetics of ion-dependent protein folding by time-resolved NMR spectroscopy at atomic resolution. J Am Chem Soc 122:6169–6174

Kwon OY, Kwon IC, Song HK, Jeon H (2008) Real-time imaging of NF-AT nucleocytoplasmic shuttling with a photoswitchable fluorescence protein in live cells. Biochim Biophys Acta 1780:1403–1407

Mal TK, Masutomi Y, Zheng L, Nakata Y, Ohta H, Nakatani Y, Kokubo T, Ikura M (2004) Structural and functional characterization on the interaction of yeast TFIID subunit TAF1 with TATA-binding protein. J Mol Biol 339:681–693

Mizuno H, Mal TK, Wälchli M, Kikuchi A, Fukano T, Ando R, Jeyakanthan J, Taka J, Shiro Y, Ikura M, Miyawaki A (2008) Light-dependent regulation of structural flexibility in a photochromic fluorescent protein. Proc Natl Acad Sci USA 105:9927–9932

Mizuno H, Dedecker P, Ando R, Fukano T, Hofkens J, Miyawaki A (2010) Higher resolution in localization microscopy by slower switching of a photochromic protein. Photochem Photobiol Sci 9:239–248

Mok KH, Hore PJ (2004) Photo-CIDNP NMR methods for studying protein folding. Methods 34:75–87

Nam KH, Kwon OY, Sugiyama K, Lee WH, Kim YK, Song HK, Kim EE, Park SY, Jeon H, Hwang KY (2007) Structural characterization of the photoswitchable fluorescent protein Dronpa-C62S. Biochem Biophys Res Commun 354:962–967

Rubinstenn G, Vuister GW, Mulder FA, Düx PE, Boelens R, Hellingwerf KJ, Kaptein R (1998) Structural and dynamic changes of photoactive yellow protein during its photocycle in solution. Nat Struct Biol 5:568–570

Rubinstenn G, Vuister GW, Zwanenburg N, Hellingwerf KJ, Boelens R, Kaptein R (1999) NMR experiments for the study of photointermediates: application to the photoactive yellow protein. J Magn Reson 137:443–447

Scheffler JE, Cottrell CE, Berliner LJ (1985) An inexpensive, versatile sample illuminator for photo-CIDNP on any NMR spectrometer. J Magn Reson 63:199–201

Shroff H, Galbraith CG JA, White Helen, Gillette J, Olenych S, Davidson MW, Betzig E (2007) Dual-color superresolution imaging of genetically expressed probes within individual adhesion complexes. Proc Natl Acad Sci USA 104:20308–20313

Spera S, Bax A (1991) Empirical correlation between protein backbone conformation and Ca and Cb nuclear magnetic resonance chemical shifts. J Am Chem Soc 113:5490–5492

Stiel AC, Trowitzsch S, Weber G, Andresen M, Eggeling C, Hell SW, Jakobs S, Wahl MC (2007) 1.8 Å bright-state structure of the reversibly switchable fluorescent protein Dronpa guides the generation of fast switching variants. Biochem J 402:35–42

Ward HR, Lawler RG (1967) Nuclear magnetic resonance emission and enhanced apsorption in rapid organometallic reactions. J Am Chem Soc 89:5518–5519

Wilbur DJ, Allerhand A (1976) Titration behavior of individual tyrosine residues of myoglobins from sperm whale, horse, and red kangaroo. J Biol Chem 251:5187–5194

Wilmann PG, Turcic K, Battad JM, Wilce MC, Devenish RJ, Prescott M, Rossjohn J (2006) The 1.7 Å crystal structure of Dronpa: a photoswitchable green fluorescent protein. J Mol Biol 364:213–224

Wishart DS, Sykes BD (1994) The ^{13}C chemical-shift index: a simple method for the identification of protein secondary structure using ^{13}C chemical-shift data. J Biomol NMR 4:171–180